Ocean Engineering 150 (2018) 21–35

Contents lists available at ScienceDirect

Ocean Engineering

journal homepage: www.elsevier.com/locate/oceaneng

Impedance functions for rigid skirted caissons supporting offshore wind turbines

Saleh Jalbi, Masoud Shadlou, S. Bhattacharya *

University of Surrey, United Kingdom

ARTICLE INFO

Keywords:
Suction caissons
Impedance functions
Natural frequency
Offshore wind turbines

ABSTRACT

Large diameter caissons are being considered as plausible foundations for supporting offshore wind turbines (OWTs) where reductions in overall cost and environmentally friendly installation methods are expected. The design calculations required for optimization of dimensions/sizing of such caissons are critically dependent on the foundation stiffness as it is necessary for SLS (Serviceability Limit State), FLS (Fatigue Limit State), and natural frequency predictions. This paper derives closed form expressions for the 3 stiffness terms (Lateral stiffness K_L, Rotational Stiffness K_R and Cross-Coupling term K_{LR}) for suction caissons having aspect ratio between 0.5 and 2 (i.e. $0.5 < L/D < 2$) which are based on extensive finite element analysis followed by non-linear regression. The derived stiffness terms are then validated and verified using studies available in literature. An example problem is taken to demonstrate the application of the methodology.

1. Introduction and background literature

With the growing interest and demand for renewable energy, larger wind turbines are used and installed in deeper waters. Fig. 1(a) shows a schematic diagram of the current and future wind turbine dimensions. Two important points may be noted:

(a) The hub height is increasing due to the large rotor diameter. This leads to the fact that not only does the dead load increase but more importantly the lateral loads and overturning moments will also increase. In fact, the governing load for foundation design is the large overturning moment.
(b) With increasing tower height and a heavier RNA (Rotor-Nacelle-Assembly) mass, the overall structure becomes more flexible and the target natural frequency for the so-called "*soft-stiff*" design shifts towards the wave frequency, see Fig. 1(b). For example, a typical 8 MW turbine will have a target frequency of 0.2 Hz which is very close to the predominant North Sea wave frequency of 0.1 Hz. This is even more challenging for Chinese Wind Farm developments as the predominant wave frequency for Bohai sea and the Yellow sea is 0.2 Hz, (Bhattacharya et al., 2017).

The above calls for optimized design and more importantly critical dynamic considerations. Monopiles are currently the most preferred foundations supporting 81% of Europe's OWTs (about 2900 turbines). However, there are multiple problems associated with monopiles of very large diameter (often known as XL piles) and the most obvious are the additional costs associated with material, manufacturing, transportation, and installation. Installation in particular poses numerous difficulties such as the risk of buckling of pile tip with very thin wall, large hammer requirements, and drilling requirement in the midst of driving (i.e. drill-drive-drill operation). These piles are hammered in dense sand or weathered bed rock, and several cases have been reported in the offshore oil and gas industry where large steel piles have collapsed during driving due to the progression of lateral deformations (Bhattacharya et al., 2005; Aldridge et al., 2005). Furthermore, there is a scarcity of installation barges required for driving piles of such large sizes which not only increases project costs but also construction delays. Apart from the engineering challenges, there are environmental issues: noise pollution caused by pile driving harms the marine life. German authorities impose regulations on pile driving noise (160 dB at 750 m distance) and it is expected to be adopted by other European nations in the near future (Müller and Zerbs, 2011). While measures may be adopted to limit noise pollution (such as the use of bubble curtains or sleeves), the success is limited (Golightly, 2014). In this context, it is important to state that foundations constitute about 34% of the overall cost of a wind farm mainly due to the stiffness requirements (Bhattacharya, 2013), and any innovation in this field can yield significant advantages.

* Corresponding author.
E-mail address: S.Bhattacharya@surrey.ac.uk (S. Bhattacharya).

https://doi.org/10.1016/j.oceaneng.2017.12.040
Received 5 June 2017; Received in revised form 26 October 2017; Accepted 17 December 2017

Nomenclature

L:	Foundation Depth	t	Foundation thickness
D	Foundation Diameter	ρ	Foundation head deflection
R	Foundation Radius	θ	Foundation head rotation
Pile:	Foundation with L/D > 2	I_p:	Foundation second moment of area
Caisson	Foundation with 0.5 < L/D < 2	I_T	Tower second moment of area
E_{SO}	initial soil Young's modulus at 1D depth	f_0	First natural frequency (flexible)
E_S	Vertical distribution of soil's Young's modulus	f_{FB}	Fixed base (cantilever) natural frequency
G_{SO}	initial soil shear modulus at 1R depth	C_L,C_R	Lateral and rotational flexibility co-efficient
υ_s	Soil Poisson's ratio	m_{RNA}	Mass of Rotor Nacelle assembly
K_L:	Lateral stiffness of the foundation	m_T	Mass of tower
K_{LR}	Cross-coupling stiffness of the foundation	C_{MP}	Substructure flexibility co-efficient
K_R	Rotational Stiffness of the foundation	D_b	Tower bottom diameter
E_p:	Foundation Young's modulus	D_t	Tower top diameter
M	Applied moment at foundation head	D_T	Average tower diameter
H	Applied lateral load at foundation head	t_T	Tower wall thickness
		Ψ	Length ratio
		χ	Bending stiffness ratio

Large diameter suction caissons are currently being considered as an alternative to monopiles for water depths of 30 m and less. These foundations consist of a rigid circular lid with thin skirts (Fig. 2) and have been primarily used as anchors in the oil and gas industry. Extensive research has been conducted on the use of skirted suction caissons to support OWTs in sand and clays under different loading conditions where Houlsby et al. (2005) and Cox and Bhattacharya (2016) presented scaled model tests, numerical modelling and general comprehensive findings for feasibility. The installation of such foundation consists of allowing the caisson to sink under its own weight and then achieving full depth of penetration by pumping the trapped water out and also by creating a pressure difference. This method can arguably reduce noise pollution

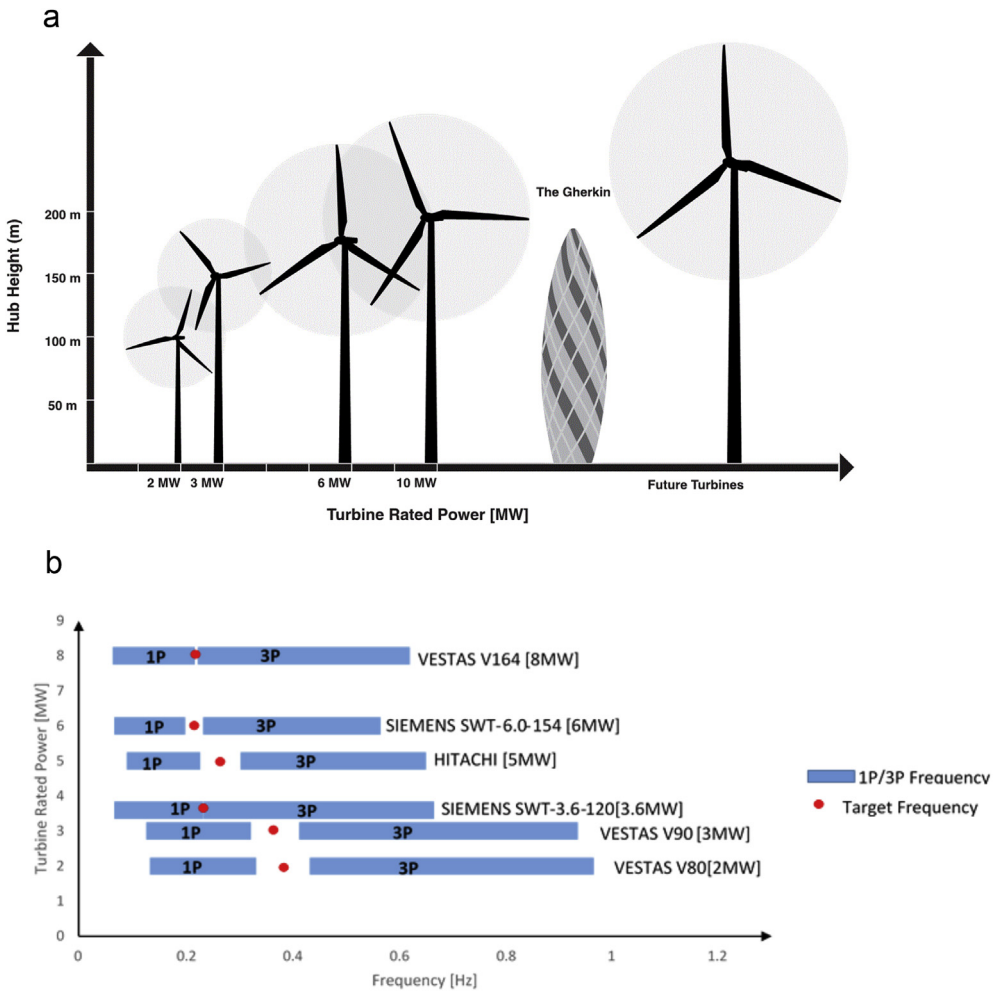

Fig. 1. (a): Current and Future OWTs. (b) Shift in target frequency.

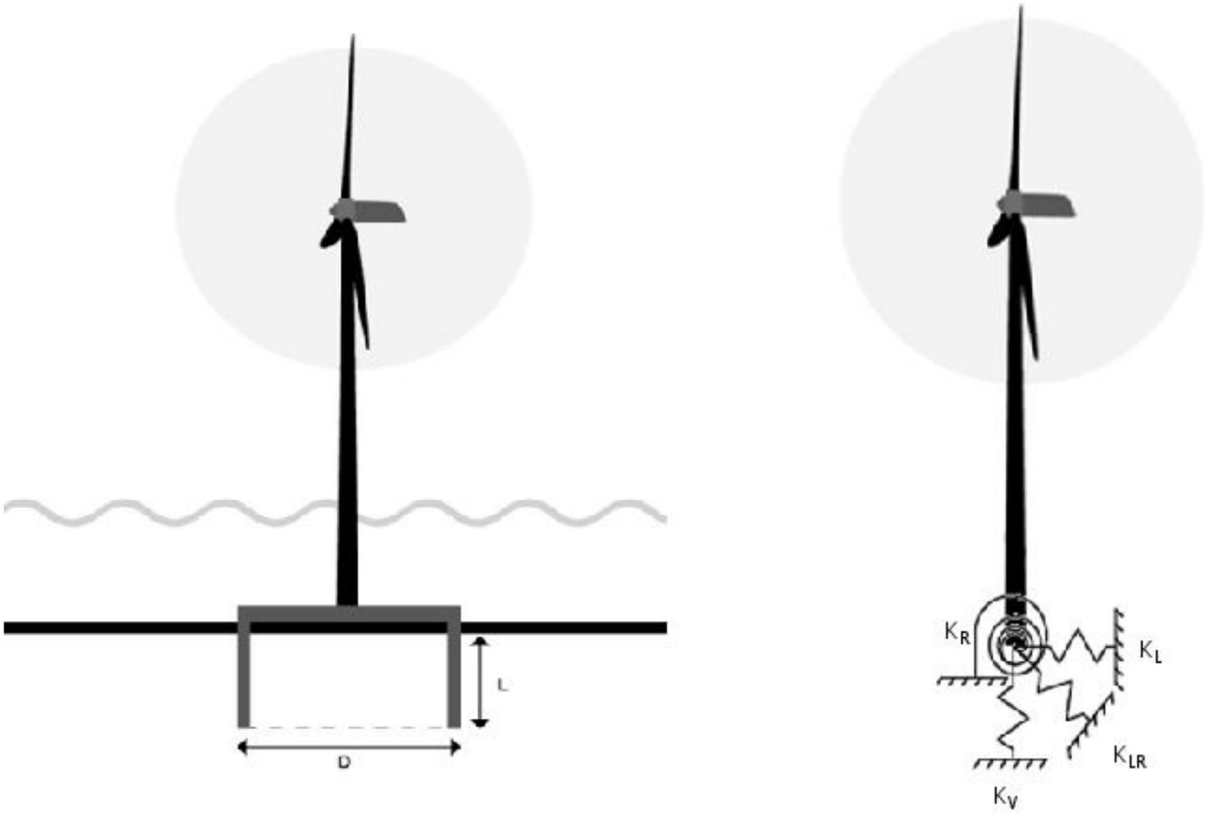

Fig. 2. (a): Caisson supported OWT (Physical problem); (b): Mechanical Representation of the Foundation.

associated with installation. Moreover, some studies suggested caisson foundations are less prone to scouring effects as compared to monopiles, see Whitehouse (2004) and Stroescu et al. (2016). In summary, there seems to be numerous reasons to investigate the use of caissons as supports to OWTs. Caissons have been previously used as supports to OWTs firstly as a trial in Frederikshavn (Denmark in 2002), followed by a caisson installed at the Horns Rev II site in 2009 and further two at the Dogger Bank site in 2013 with aspect ratios (L/D) between 0.5 and 1 (Stroescu et al., 2016). However, as turbine sizes are increasing it is expected that caissons required to support such structures will also increase in size.

It is important to emphasise the distinction between embedded and skirted foundations. While skirted foundations trap soil mass below the lid and with the enclosed area, embedded foundations are either fully solid, or rest directly on the soil, such as surface foundations with or without backfill. Following the dynamic calculation methods proposed by Adhikari and Bhattacharya (2012) and improved version presented in Arany et al. (2016) and Arany et al. (2017), foundation stiffness can be represented by a mechanical model shown in Fig. 2(b) through a set of springs: Lateral stiffness (K_L), Rotational stiffness (K_R), Cross-Coupling stiffness (K_{LR}) and vertical stiffness (K_V). As the system is infinitely stiff vertically, no vibration is expected in that direction, hence K_V can be ignored in calculations. Extensive research from the field of machine foundations provides sufficient information regarding the elastic static and dynamic stiffness values of embedded foundations and rigid circular footings in a homogeneous soil, see for example Gazetas, (1983), Gazetas (1991), and Poulos and Davis (1974). Generally, most literature reports that stiffness decreases with increasing strains and increasing forcing frequencies. However, research on elastic and non-linear stiffness of a skirted caisson is limited. Doherty et al. (2005) used FEA to provide tabulated coefficients for computing the elastic stiffness. The analyses were carried out using variations of Poisson's ratio, skirt embedment, and relative skirt to soil stiffness in homogeneous, linear, and parabolic ground profiles. The values were presented as tabular coefficients which can be used for preliminary foundation sizing as the authors provide coefficients for numerous cases and recommended interpolation within the values. This can be a suitable method to check obtained results. Recently, Gelagoti et al. (2015) used mathematical operations to convert the spring stiffness of a shallow embedded foundation suggested by Gazetas (1983) to a skirted caisson. The aforementioned research also shows that the stiffness value of a rigid caisson and a rigid embedded foundations are very similar. It also discusses the effect of skirt flexibility and strain level on the impedance values. However, the authors only provide solutions for homogeneous soils. Finally, Latini and Zania (2017) studied the dynamic lateral response of suction caissons and presented an equation which provides a good estimate of the elastic deflection and rotation of a suction caisson. However, these equations cannot be used for simplified dynamic calculations.

In the context of foundation stiffness previous work on deep foundations was carried out by Randolph (1981), Carter and Kulhawi (1992), and Higgins and Basu (2011) through FEA analysis for rigid and flexible piles in homogeneous and linear inhomogeneous soils. Recently, Shadlou and Bhattacharya (2016) presented impedance functions for rigid deep foundations in homogeneous, parabolic, and linear ground profiles (Table 1) keeping in mind the application for offshore wind turbines. From these studies, it can be noted that the driving analysis parameters for rigid foundations are: aspect ratio (L/D), Soil stiffness at one diameter below the ground (E_{SO}) and Poisson's ratio of the soil (υ_s) which were the variables used to obtain closed form solutions for K_L, K_R, and K_{LR} for rigid caissons. It may also be noted that the impedance functions presented in Table 1 are applicable for L/D greater than 2.

Identifying the gap in the literature and focusing on the future offshore developments, the aims of the paper are as follows:

(a) Providing closed form solutions for rigid caissons of aspect ratio between 0.5 and 2 i.e. $0.5 < L/D < 2$ in three types of ground: homogeneous, parabolic and linear profiles.

Table 1
Impedance functions for deep foundations exhibiting rigid behaviour L/D > 2.

$f(\upsilon_s) = 1 + 0.6|0.25 - \upsilon_s|$

Ground profile See Fig. 4 for definition	$\frac{K_L}{DE_{SO}f(\upsilon_s)}$	$\frac{K_{LR}}{D^2E_{SO}f(\upsilon_s)}$	$\frac{K_R}{D^3E_{SO}f(\upsilon_s)}$
Homogeneous	$3.2\left(\frac{L}{D}\right)^{0.62}$	$-1.8\left(\frac{L}{D}\right)^{1.56}$	$1.65\left(\frac{L}{D}\right)^{2.5}$
Parabolic	$2.65\left(\frac{L}{D}\right)^{1.07}$	$-1.8\left(\frac{L}{D}\right)^{2}$	$1.63\left(\frac{L}{D}\right)^{3}$
Linear	$2.35\left(\frac{L}{D}\right)^{1.53}$	$-1.8\left(\frac{L}{D}\right)^{2.5}$	$1.59\left(\frac{L}{D}\right)^{3.45}$

(b) Demonstrate the application of the methodology by taking an example. The stiffness parameter can be used for natural frequency estimates and in some cases (within elastic range) SLS outputs such as foundation rotation and deflections can be predicted.

It must be mentioned that these solutions can be used for preliminary sizing of caisson at feasibility and tender design stage. Once the size is optimized and project finalised, further optimization and detailed analysis should be carried out using conventional methods.

2. Numerical modelling

2.1. Methodology

Finite element method PLAXIS 3D has been used in this study where the soil is modelled as linear elastic material since only the stiffness at small strains is required. This assumption is valid as the natural frequency is concerned with very small amplitude of vibrations and the prediction of the initial stiffness would suffice (Arany et al., 2017). Similarly studies on the dynamic stiffness by Shadlou and Bhattacharya (2016) regarding rigid deep foundations show that for very low frequency applications (such as wind turbines) the static and dynamic stiffness are almost similar and the effect of the forcing frequency on the stiffness values can be ignored. Likewise Latini and Zania (2017) reported results on suction caissons and a similar response was noted. Moreover, a "Rigid Body" has been set to the foundation where it is not allowed to deform or bend, and only the surrounding soil is mobilized. This assumption is also valid especially in soft soils as the caisson has a low aspect ratio and also because steel has higher flexural and shear stiffness than soil. The interface between the soil and foundation had the same stiffness properties as the surrounding soils and a very fine mesh was implemented for enhanced accuracy. As the material model is linear elastic (strength was not specified) no slip or gapping between the soil and structure elements was modelled and a rigid contact is maintained between them. This assumption was implemented in the procedure as the main intention of the impedance functions is to obtain the Eigen Frequency of the system and so elasticity must be maintained and in effect this is elasto-dynamic solution. In reality, some gapping may occur between the skirt and surrounding soil, however as the natural frequency is concerned with small amplitude vibrations, gapping may be ignored for preliminary analysis.

The extent of the soil contour was taken as 20D (D = 5.0 m) and the depth h (h is the depth of the soil stratum) was at least twice that of the foundation. The objective was to ensure the stresses in the soil are not affected by the proximity of the translational boundary conditions at the end and bottom faces. Previous work presented in Krishnaveni et al. (2016) modelled the stratum with 5D width, whilst Abbas et al. (2008) used 40D on finite element software to analyse laterally loaded piles, which shows a wide gap of possibilities. PLAXIS 3D also allows the user to define either a constant stiffness or stiffness increasing linearly with depth. These two options were utilized to model homogenous and linear ground profiles, respectively. For parabolic variation of soil stiffness, the soil stratum was discretized with multiple layers where each layer had of depth 0.025 h. An initial stiffness value and linear slope was input to each layer to represent a parabolic stiffness variation (Figs. 3–4). Homogeneous soils are soils which have a constant stiffness with depth such as over-consolidated clays. On the other hand, a linear profile is typical for normally consolidated clays (or "Gibson Soil" (Gibson, 1974)) and parabolic behaviour can be used for sandy soils. The density assigned to all ground profiles was 18 kN/m^3. To save computational power and operational time cost, only half the system was modelled due to symmetry. The software also has the capability to model the initial stresses in the stratum and the change in the stress state due to the construction sequence where in a linear elastic soil model, the user can change the k_0 value. In this study, the k_0 value set was the default value of 1. Accordingly, the displacements were set to zero prior to application of the loads and values for K_L, K_R, and K_{LR} were computed. The process by which this is done is shown in the appendix.

2.2. Methodology verification and comparison of results

Based on the methodology presented in the earlier section, results were obtained by plotting normalized values for K_L, K_R, and K_{LR} against L/D for $0.2 < L/D < 10$ where $\upsilon_s = 0.2$ for homogeneous and linear inhomogeneous ground profiles (Fig. 5(a)). The results are compared with Shadlou and Bhattacharya (2016) closed form solutions which in turn were coherent with Higgins and Basu (2011) flexibility functions. Similarly, results for homogeneous ground profiles at $\upsilon_s = 0.499$ are presented in appendix A.3 to show the applicability of the extraction method of a practical range of Poisson's ratio. Moreover, table in appendix A.2 summarizes all the cases simulated in this study.

Fig. 5 show a good match with literature for K_L and K_{LR} most L/D values included in the study, specifically L/D > 2 (deep foundations), hence available closed form solutions for deep foundations can still be applied in that range. Moreover, the coherence between the extracted results and literature for L/D > 2 justifies the method of extraction, the mesh used, the extent of the boundary conditions, and the rigid body assumption applied in the finite element model. However, it may be observed that there are some discrepancies in K_R where differences arise for $L/D < 2$. A closer look is shown where only values of $0.2 < L/D < 2$ are plotted in Fig. 6.

From Fig. 6 the K_R value predicted by PLAXIS 3D for foundations of low L/D seems to be stiffer than by the closed form solutions presented by Shadlou and Bhattacharya (2016). Current impedance functions that were intended for deep foundations do not accurately predict the rotational stiffness at low aspect ratios, and according to Arany et al. (2015) the rotational stiffness is one of the most dominant variables in natural frequency estimation. Thus, due to the differences in K_R shown above, it is necessary to have a separate impedance functions for rigid skirted caissons ($L/D < 2$) in order to have enhanced estimates of the natural frequency of a caisson supported offshore wind turbine.

The effect of Poisson's ratio on stiffness terms was also noted from the FE analysis. Fig. 7 presents the effect of Poisson's ratio on the lateral foundation stiffness in a homogeneous ground profile where these results were normalized against $\upsilon_s = 0.1$. FE analysis shows that the stiffness decreases with increasing υ_s until $\upsilon_s = 0.4$ and then slightly increases. Moreover, the aspect ratio L/D influences the effect of υ_s where different reduction values were recorded for L/D = 6, 4, and 1 respectively. Previous literature such as Shadlou and Bhattacharya (2016) suggest an absolute value function whilst Gazetas (1983) and Doherty et al. (2005) suggested a linear increase of stiffness with Poisson's ratio. It is also noteworthy to state that the impact of Poisson's ratio on foundation stiffness predicted by this study, Shadlou and Bhattacharya (2016) and Randolph (1981) are lower than Gazetas, (1983) and Doherty et al. (2005). In most practical cases, the soil Poisson's ratio lies between 0.25 and 0.5 and according to Fig. 7, there is a noticeable reduction in lateral stiffness which and so an optimized correction factor f (υ_s), which depends on both υ_s and L/D will be introduced for K_L, K_{LR}, and K_R.

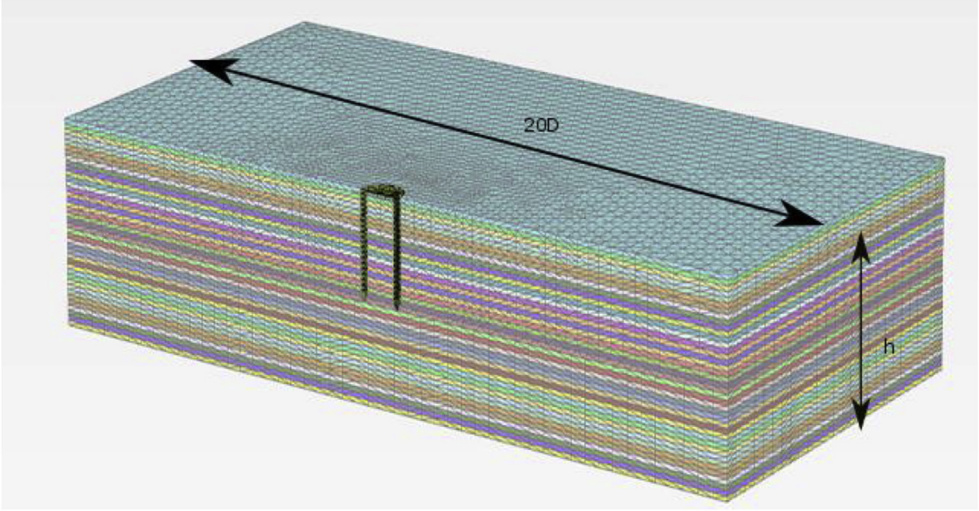

Fig. 3. Soil model used to simulate parabolic stiffness variation in PLAXIS 3D.

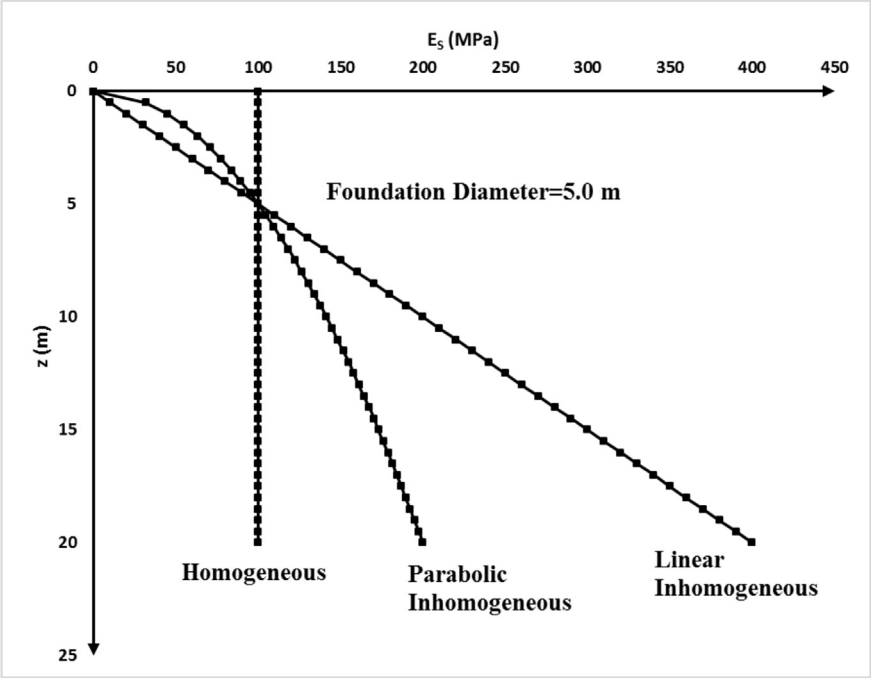

Fig. 4. Stiffness variation with depth.

2.3. Development of the impedance functions and correction factors

A non-linear regression analysis was performed on a normalized set of samples to obtain close form solutions. The diameter was kept constant at 5 m, and the soil stiffness was set as 100 MPa at 5 m depth (1 Diameter depth) as shown in Fig. 4. The study then plots the change of K_L, K_R, and K_{LR} with increasing L (L values include 2.5 m,5 m,7.5 m, and 10 m) and υ_s (0.1–0.49). First, a new correction due to Poisson's ratio will be presented that can be applied for $0.5 < L/D < 6$. The reason this study was performed up to $L/D = 6$ is to clarify how the Poisson ratio affects the stiffness values at different ranges of embedded foundations. Hence, Fig. 7 shows that the Poisson ratio correction function $f(\upsilon_s)$ extracted from the finite element analysis is not only a function of the Poisson's ratio itself, but also a function of L/D, which has not been previously addressed in literature where the correction factors are only dependent on the magnitude of υ_s, and so revised correction factors $f(\upsilon_s)$ dependent on both υ_s and L/D are required. From Fig. 7, it is clear that the best fit function would be a polynomial in the form of $f(\upsilon_s) = a_0\upsilon_s^2 - a_1\upsilon_s + a_2$ The values for a_0, a_1, and a_2 for $L/D = 1$, 4, and 6 were obtained and normalized against $L/D = 6$. The values for $L/D = 6$ are $a_0 = 1.1017$, $a_1 = -0.6964$, $a_2 = 1.0599$. Fig. 8 shows the normalized values a_0, a_1, and a_2. It is evident that a_0 is the only parameter that is affected by L/D and is also given a best fit 2nd order polynomial function. Hence the correction due to Poisson's ratio can be summarized as

$$f(\upsilon_s) = 1.1017\alpha\upsilon_s^2 - 0.6964\upsilon_s + 1.0599 \tag{1a}$$

Where

$$\alpha = -0.0048\left(\frac{L}{D}\right)^2 + 0.0962\left(\frac{L}{D}\right) + 0.5941 \tag{1b}$$

This can be further simplified to:

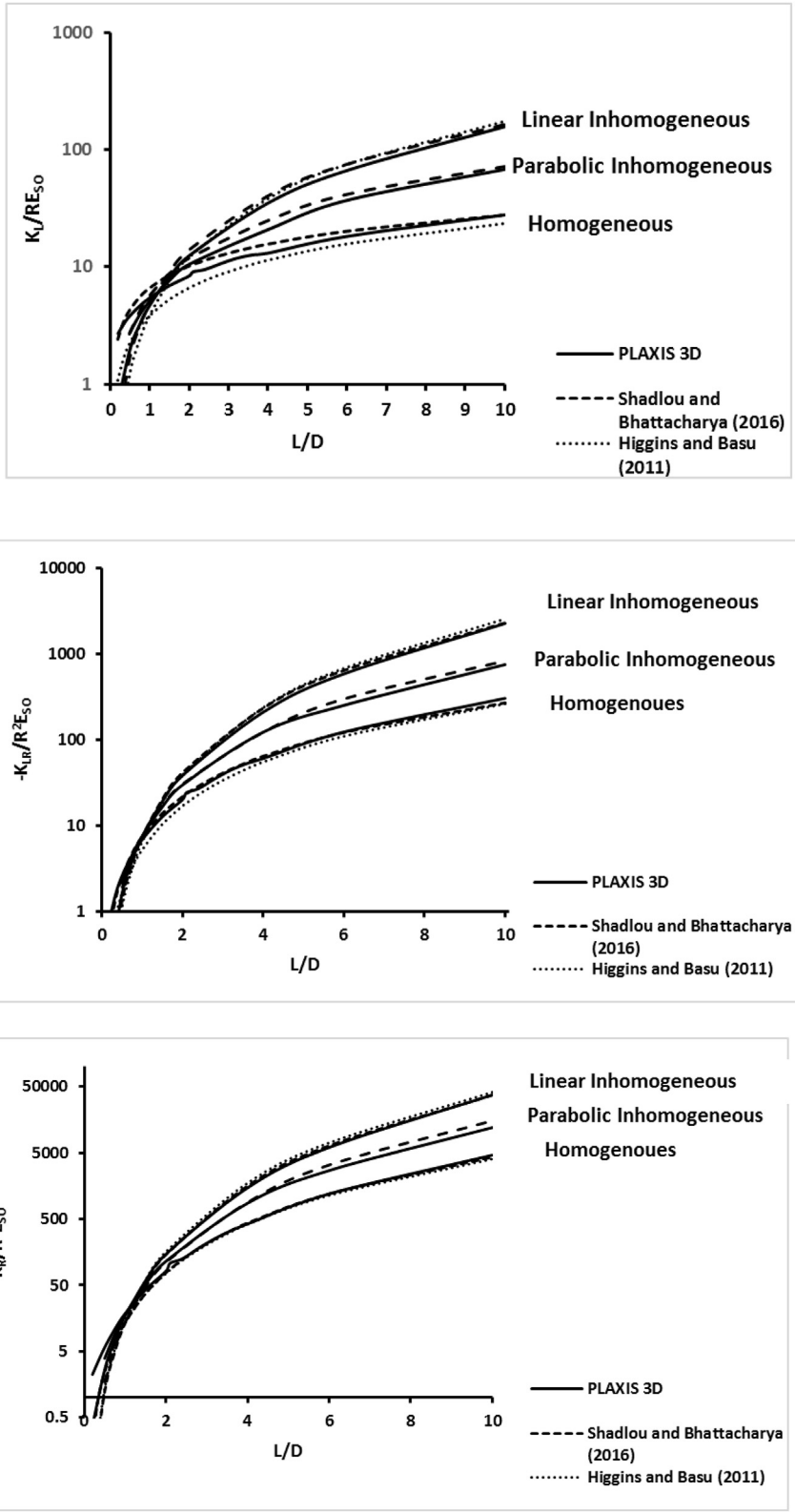

Fig. 5. Impedance functions for foundations exhibiting rigid behaviour for Homogeneous, Linear Inhomogeneous, and Parabolic Inhomogeneous Ground Profiles.

$$f(\upsilon_s) = 1.1 \times \left(0.096\left(\frac{L}{D}\right) + 0.6\right)\upsilon_s^2 - 0.7\upsilon_s + 1.06 \quad (1c)$$

Thus, according to Eqn (1c), f (υ_s) is affected by both L/D and υ_s. It must be noted that the same methodology was repeated for K_L, K_R, and K_{LR} in parabolic and linear inhomogeneous ground profiles where the f (υ_s) formulation obtained in each case was very similar to the one presented in equation (1c). For instance, Fig. 9 shows how similar values of a_0 was obtained for the three stiffness terms. Moreover, there was no noticeable change when the formula was also used for different lower aspect ratios of L/D < 1.

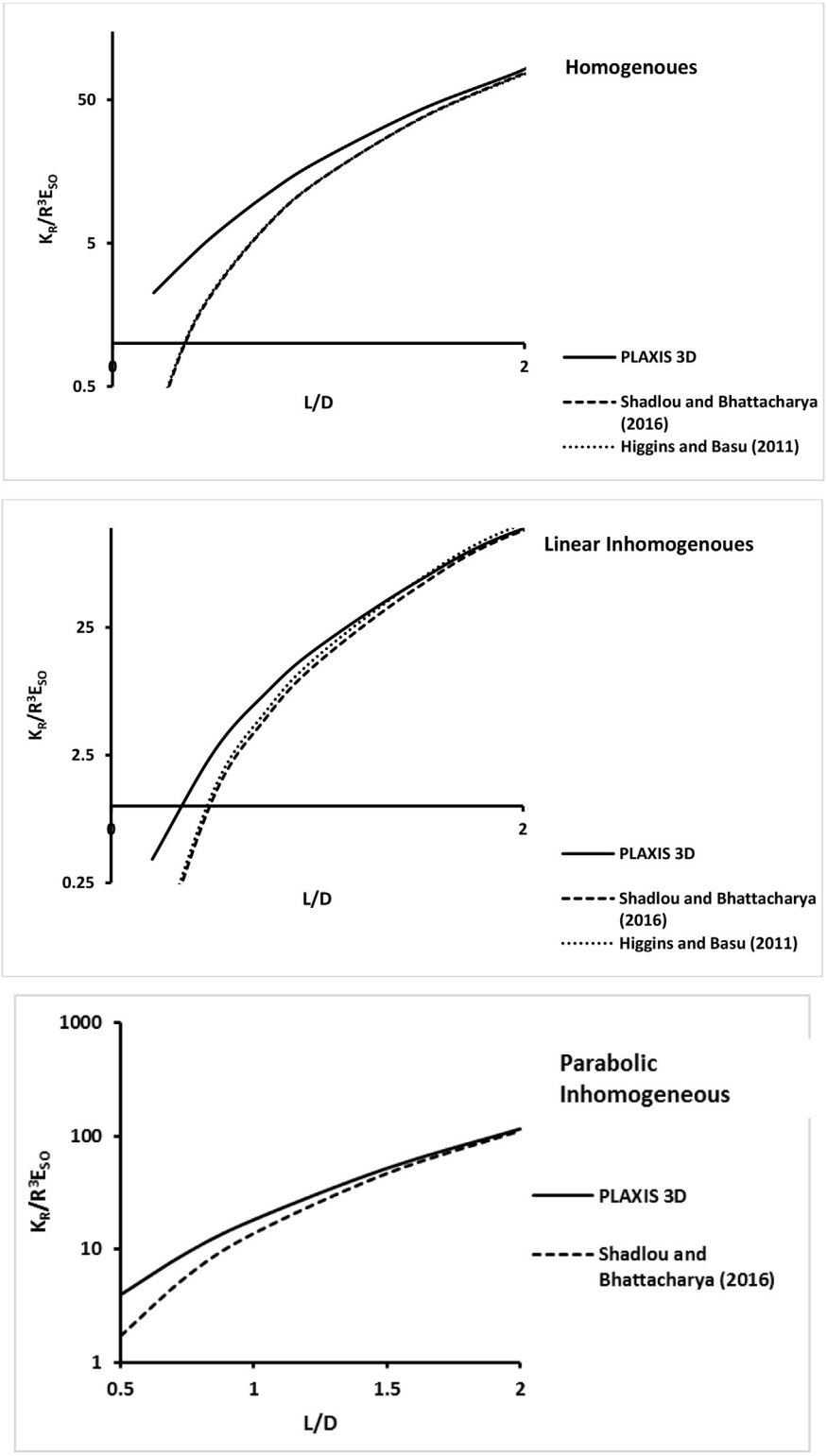

Fig. 6. Rotational impedance functions for $0.5 < L/D < 2$.

3. Proposed impedance functions for rigid skirted caissons

The normalized values of $\frac{K_L}{RE_{SO}\bar{f}(\upsilon_s)}$, $\frac{K_{LR}}{R^2E_{SO}\bar{f}(\upsilon_s)}$, $\frac{K_R}{R^3E_{SO}\bar{f}(\upsilon_s)}$ were computed and plotted against L/D for all ground profiles. Consequently, best fit power functions were derived using a spreadsheet program. One may note that previous literature has also used power functions and the R^2 values presented show it is still applicable for shallow rigid caissons. For brevity, Fig. 10 only plots results for homogeneous ground profile.

Table 2 provides the impedance functions for Rigid Skirted Caissons for $0.5 < L/D < 2$ in 3 ground profiles. For practicality, the values were presented in terms of foundation diameter D.

As stated above there is a close similarity for K_L and K_{LR} values and the difference between K_R values which have higher multipliers for the caisson when compared to deep foundations, as shown when comparing K_R values in Tables 1 and 2, or clearly shown in Fig. 10.

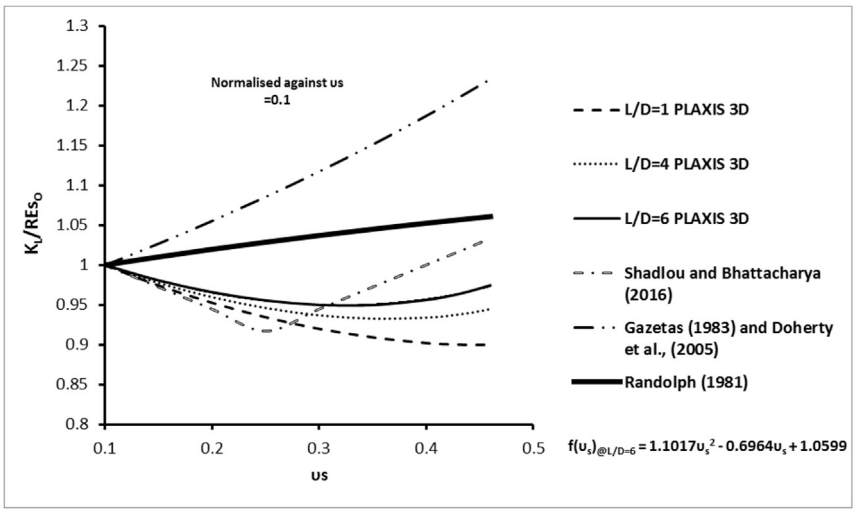

Fig. 7. Variation of lateral stiffness (K_L) with Poisson's ratio (υ_s).

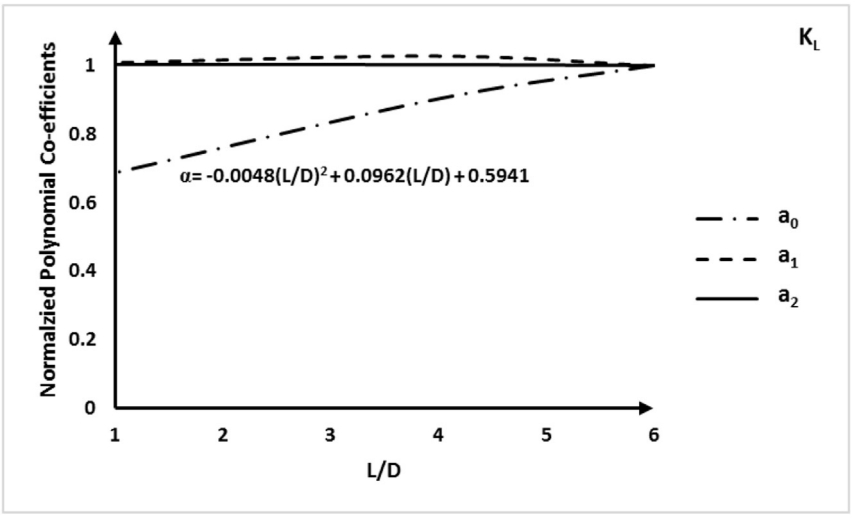

Fig. 8. Variation of a_0,a_1, and a_2 with L/D.

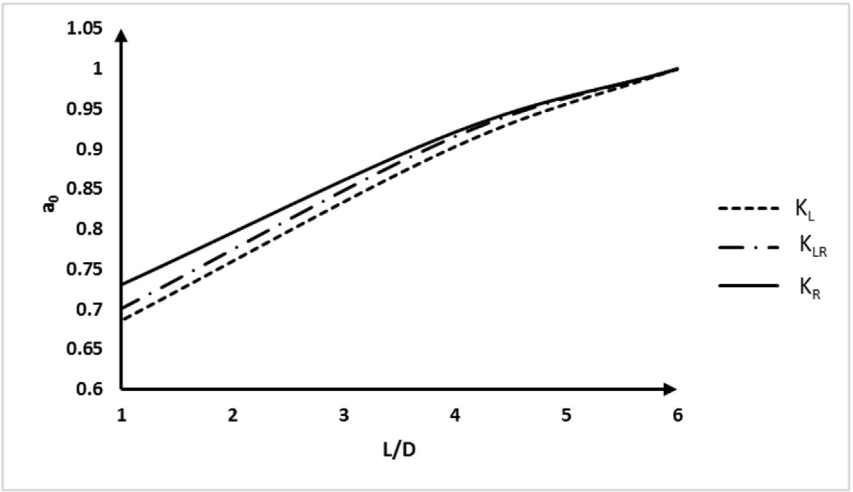

Fig. 9. Variation of a_0 for K_L K_{LR} and K_R.

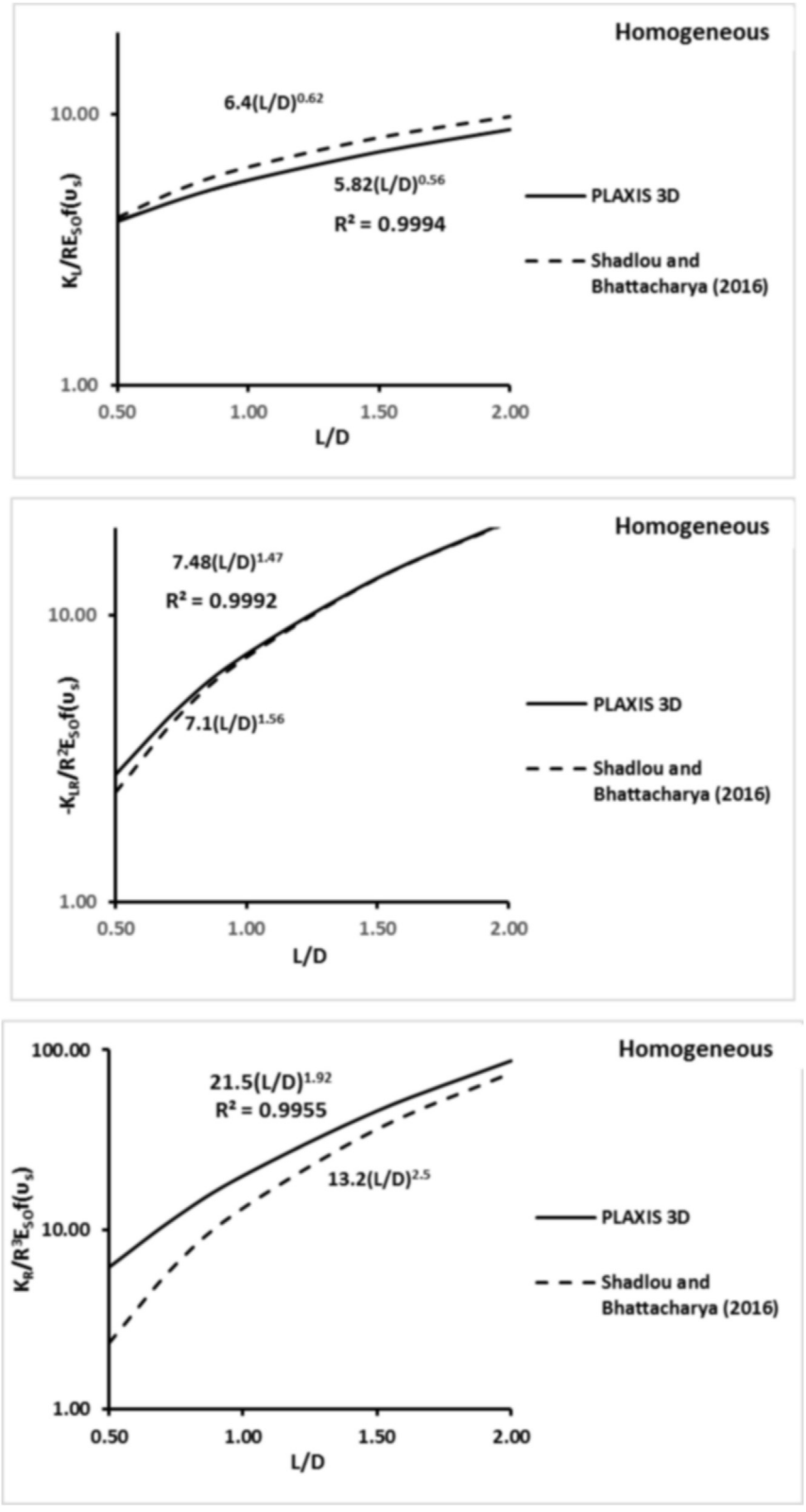

Fig. 10. Best fit curves for impedance functions (Homogeneous).

4. Discussion and validation of the results

The impedance functions provided in Table 2 were used to calculate K_L, K_R, and K_{LR} for the cases simulated using PLAXIS 3D. The highest recorded percentage difference was 10%. In the context of natural frequency estimation, this error will only lead to 2–3% error in prediction of the natural frequency following the Arany et al. (2016) formulation. The results were also checked against the co-efficients provided for Rigid caissons by Doherty et al. (2005) and summarized in Table 3(a) and 3(b). To allow comparison, it may be noted that the results presented have been normalized against G_{SO} which is the shear modulus at depth of D/2 as laid out in Doherty et al. (2005).

Table 2
Impedance functions for shallow skirted foundations exhibiting rigid behaviour $0.5 < L/D < 2$.

$$f(\upsilon_s) = 1.1 \times \left(0.096\left(\frac{L}{D}\right) + 0.6\right)\upsilon_s^2 - 0.7\upsilon_s + 1.06$$

Ground profile	$\frac{K_L}{DE_{SO}f(\upsilon_s)}$	$\frac{K_{LR}}{D^2E_{SO}f(\upsilon_s)}$	$\frac{K_R}{D^3E_{SO}f(\upsilon_s)}$
Homogeneous	$2.91\left(\frac{L}{D}\right)^{0.56}$	$-1.87\left(\frac{L}{D}\right)^{1.47}$	$2.7\left(\frac{L}{D}\right)^{1.92}$
Parabolic	$2.7\left(\frac{L}{D}\right)^{0.96}$	$-1.99\left(\frac{L}{D}\right)^{1.89}$	$2.54\left(\frac{L}{D}\right)^{2.44}$
Linear	$2.53\left(\frac{L}{D}\right)^{1.33}$	$-2.02\left(\frac{L}{D}\right)^{2.29}$	$2.46\left(\frac{L}{D}\right)^{2.9}$

The following can be concluded from the analysis: (a) The proposed method showed good agreement with Shadlou and Bhattacharya (2016) for $L/D > 2$; (b) The closed form solution showed an acceptable level of error when compared to the original results from PLAXIS 3D, showing that the power function and Poisson's ratio corrections are acceptable; (c) The results showed good correlation with tabular co-efficients provided by Doherty et al. (2005) for a wide range of Poisson's ratios. It may be noted that the difference in results is higher when a linear soil profile is taken. Moreover, Doherty et al. (2005) always show an increase in stiffness at low L/D ratios, whilst the closed form solutions show a decrease in stiffness at low aspect ratios when comparing homogeneous and linear ground profiles. It may be then concluded that the closed form solutions are applicable for a wide range of Poisson's ratios.

5. Application of the methodology

An example is taken to demonstrate the application of the methodology. The wind turbine used for this example is the 5 MW reference wind turbine provided by NREL, see Jonkman et al. (2009) and the details of the turbine support structure are summarized in Table 4.

The wind turbine is assumed to be placed in a homogeneous ground profile with $E_S = E_{SO} = 40$ MPa. Caisson dimensions of $L = 6$ m and $D = 12$ m is used to demonstrate the calculation method. K_L K_R and K_{LR} are calculated using Table 2 and the important steps are shown below (see Fig. 11).

For the problem $L/D = 0.5$ and being in homogeneous soil, Row 2 of Table 2 is taken.

$$f(\upsilon_s) = 1.1 \times \left(0.096\left(\frac{L}{D}\right) + 0.6\right)\upsilon_s^2 - 0.7\upsilon_s + 1.06$$
$$= 1.1 \times [0.096(0.5) + 0.6] \times 0.35^2 - (0.7 \times 0.35) + 1.06 = 0.9$$

Table 4
Details of the OWT support structure.

Top Diameter of the Tower (m)	3.87
Bottom Diameter of the Tower (m)	6.0
Wall Thickness of the Tower (mm)	27
Height of the Tower (m)	87.6
Platform height (transition piece) (m)	30
Mass of RNA (tons)	350
Mass of Tower (tons)	347.5
Rated rotor speed (rpm)	6.9–12.1

*Assume transition piece has same cross-sectional properties as the bottom diameter of the tower.

$$K_L = 2.94\left(\frac{L}{D}\right)^{0.56} DE_{SO}f(\upsilon_s) = 2.94 \times (0.5)^{0.56} \times 12 \times 40 \times 10^{-3} \times 0.9$$
$$= 0.86\frac{GN}{m}$$

$$K_{LR} = -1.87\left(\frac{L}{D}\right)^{1.47} D^2E_{SO}f(\upsilon_s)$$
$$= -1.87 \times (0.5)^{1.47} \times 12^2 \times 40 \times 10^{-3} \times 0.9 = -3.5GN$$

$$K_R = 2.7\left(\frac{L}{D}\right)^{1.92} D^3E_{SO}f(\upsilon_s) = 2.7 \times (0.5)^{1.92} \times 12^3 \times 40 \times 10^{-3} \times 0.9$$
$$= 44\frac{GNm}{rad}$$

The target frequency of the system should within 1P/3P as shown in Fig. 1(b) which is specifically between 0.2 and 0.35 Hz (Rated power in Table 4). Following the methodology of Arany et al. (2017), the fixed base natural frequency (f_{FB}) of the wind turbine is 0.26 Hz and the first natural frequency considering SSI and foundation flexibility is given by $f_0 = C_{MP} \times C_L \times C_R \times f_{FB}$ where C_L and C_R are the foundation flexibility co-efficient based on K_L, K_R, and K_{LR} values. For the problem in hand, C_{MP},C_L and C_R are calculated 0.85, 0.99, and 0.82 respectively and the first fundamental natural frequency can them be calculated as:

$f = C_L \times C_R \times f_{FB} = 0.17$ Hz. For the sake of completeness, detailed calculation are presented in Appendix-1. It may seem that the structure is

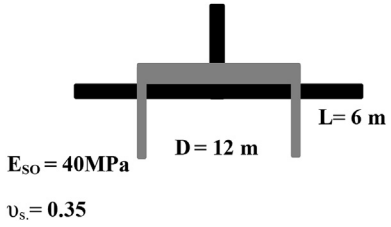

Fig. 11. Schematic of foundation dimensions and soil stiffness.

Table 3a
Comparison of K_L (Lateral Stiffness) values with Doherty et al. (2005) at $\upsilon_s = 0.2$ and $\upsilon_s = 0.4999$.

Case		$\frac{K_L}{RG_{SO}}$(Doherty et al., 2005)	$\frac{K_L}{RG_{SO}}$ (Proposed method)		$\frac{K_L}{RG_{SO}}$(Doherty et al., 2005)	$\frac{K_L}{RG_{SO}}$ (Proposed method)
L/D = 0.5 Homogeneous	$\upsilon_s = 0.2$	9.09	9.08	$\upsilon_s = 0.4999$	10.95	10.64
L/D = 0.5 Linear		10.55	9.20		13.07	10.80
L/D = 2 Homoeneous		18.04	19.87		22.61	24.41
L/D = 2 Linear		61.21	58.55		82.21	71.05

Table 3b
Comparison of K_R (Rotational Stiffness) values with Doherty et al. (2005) at $\upsilon_s = 0.2$ and $\upsilon_s = 0.4999$.

@ $\upsilon_s = 0.2$		$\frac{K_R}{R^3G_{SO}}$ (Doherty et al., 2005)	$\frac{K_R}{R^3G_{SO}}$ (Proposed method)		$\frac{K_R}{R^3G_{SO}}$ (Doherty et al., 2005)	$\frac{K_R}{R^3G_{SO}}$ (Proposed method)
L/D = 0.5 Homogeneous	$\upsilon_s = 0.2$	16.77	13.1	$\upsilon_s = 0.4999$	20.06	15.21
L/D = 0.5 Linear		17.15	12.01		21.99	14.05
L/D = 2 Homoeneous		201.6	187.41		267.3	227.64
L/D = 2 Linear		774	673.7		1093.5	818.24

flexible and close to 1P frequency (Table 4). It is of interest to also check the SLS criteria.

Based on the work of Arany et al. (2017), lateral load (H) of 4 MN and over turning moment (M) of 200 MN.m can be considered as a reasonable estimate of the worst load combination for a typical site. Assuming that the foundation behaviour (Load-deflection or moment-rotation) is in the linear range, the deflections and rotations can be estimated using Equations as

$$\begin{bmatrix} H \\ M \end{bmatrix} = \begin{bmatrix} K_L & K_{LR} \\ K_{LR} & K_R \end{bmatrix} \begin{bmatrix} \rho \\ \theta \end{bmatrix} \Rightarrow \begin{bmatrix} \rho \\ \theta \end{bmatrix} = \begin{bmatrix} 0.86 & -3.5 \\ -3.5 & 44 \end{bmatrix}^{-1} \begin{bmatrix} 0.004GN \\ 0.2GNm \end{bmatrix} = \begin{bmatrix} 0.034m \\ 0.007rads \end{bmatrix}$$

The above was an explanatory example to show how the impedance functions can be used for preliminary sizing purposes. The results show that the deflection predicted of 340 mm and rotation of 0.4° may be acceptable but the design may not satisfy the natural frequency requirements and this indicates that the size of the caisson needs to be further refined.

6. Conclusion

This paper provides closed form solution for stiffness of rigid skirted caissons founded on three types of ground profile: The formulation is developed for applications related to OWTs. The methods showed good agreement with results available in literature and can be used for caisson optimization at the feasibility and tender design stage. An example problem is taken to show the application of the methodology.

Appendix

A.1 Obtaining K_L, K_R, and K_{LR} from PLAXIS 3D

A method has been proposed by Jalbi et al. (2017) to compute the three stiffness terms (K_L, K_{LR}, and K_R) from FEA. Typically, pile head load-deflection and pile head moment-rotation curves are non-linear depending on the soil type. However, the linear range of the curves can be used to estimate pile-head rotation and deflection based on Eq. (1)

$$\begin{bmatrix} H \\ M \end{bmatrix} = \begin{bmatrix} K_L & K_{LR} \\ K_{LR} & K_R \end{bmatrix} \begin{bmatrix} \rho \\ \theta \end{bmatrix} \tag{1}$$

Eq. (1) can be re-written as Eq. (2) through matrix operation where I (Flexibility Matrix) is a 2×2 matrix given by Eq. (3)

$$\begin{bmatrix} \rho \\ \theta \end{bmatrix} = [I] \times \begin{bmatrix} H \\ M \end{bmatrix} \tag{2}$$

$$I = \begin{bmatrix} I_L & I_{LR} \\ I_{RL} & I_R \end{bmatrix} \tag{3}$$

To obtain the stiffness components, one can run a numerical model for a lateral load (say $H=H_1$) with zero moment ($M = 0$) and obtain values of deflection and rotation (ρ_1 and θ_1). The results can be expressed through Eqs. (4)–(5)

$$\begin{bmatrix} \rho_1 \\ \theta_1 \end{bmatrix} = \begin{bmatrix} I_L & I_{LR} \\ I_{RL} & I_R \end{bmatrix} \times \begin{bmatrix} H_1 \\ 0 \end{bmatrix} \tag{4}$$

$$\rho_1 = H_1 \times I_L \Rightarrow I_L = \frac{\rho_1}{H_1}$$

$$\theta_1 = H_1 \times I_{RL} \Rightarrow I_{RL} = \frac{\theta_1}{H_1} \tag{5}$$

Similarly another numerical analysis can be done for a defined moment ($M = M_1$) and zero lateral load ($H = 0$) and the results are shown in. Eqs. (6)–(7)

$$\begin{bmatrix} \rho_2 \\ \theta_2 \end{bmatrix} = \begin{bmatrix} I_L & I_{LR} \\ I_{RL} & I_R \end{bmatrix} \times \begin{bmatrix} 0 \\ M_1 \end{bmatrix} \tag{6}$$

$$\rho_2 = M_1 \times I_{LR} \Rightarrow I_{LR} = \frac{\rho_2}{M_1}$$

$$\theta_2 = M_1 \times I_R \Rightarrow I_R = \frac{\theta_2}{M_1} \tag{7}$$

From the above analysis (Eqs. (4)–(7)), terms for the I matrix (Eq. (3)) can be obtained. Eq. (2) can be rewritten as Eq. (8) through matrix operation.

$$[I]^{-1} \times \begin{bmatrix} \rho \\ \theta \end{bmatrix} = \begin{bmatrix} H \\ M \end{bmatrix} \tag{8}$$

Comparing Eqs. (1) and (8), one can easily see the relation between the stiffness matrix and the inverse of flexibility matrix (I) given by Eq. (9). Eq. (10) is a matrix operation which can be carried out easily to obtain K_L, K_R and K_{LR}.

$$K = \begin{bmatrix} K_L & K_{LR} \\ K_{RL} & K_R \end{bmatrix} = I^{-1} = \begin{bmatrix} I_L & I_{LR} \\ I_{RL} & I_R \end{bmatrix}^{-1} \tag{9}$$

$$K = I^{-1} = \begin{bmatrix} \frac{\rho_1}{H_1} & \frac{\rho_2}{M_2} \\ \frac{\theta_1}{H_1} & \frac{\theta_2}{M_2} \end{bmatrix}^{-1} \tag{10}$$

Therefore, mathematically, two FEA analyses are required to obtain the three spring stiffness terms. It is important to note that the above methodology is only applicable in the linear range and therefore.

It is advisable to obtain a load-deflection and moment-rotation curve to check the range of linearity if a non-linear soil model is used. If the analysis is used beyond the linear range, deflections and rotations will be underestimated.

A.2: Table 1: Summary of the analysis performed

Ground Profiles	E_{SO} (MPa)	L/D (D = 5 m)	υ_s
•Homogeneous •Parabolic Inhomogeneous •Linear Inhomogeneous	100	0.2,0.5,0.75,1,1.5,2,4,6,8,10	0.1,0.15,0.2,0.25,0.3,0.35,0.4,0.42,0.44,0.46,0.499

A.3 K_L, K_R, and K_{LR} at $\upsilon_s = 0.499$

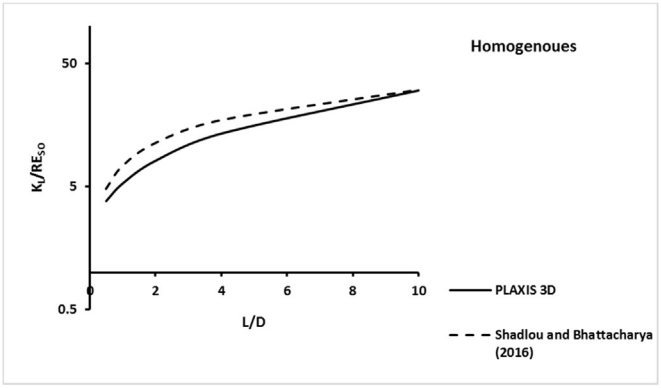

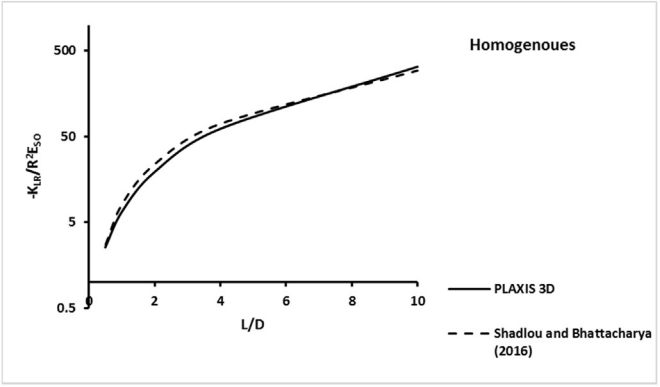

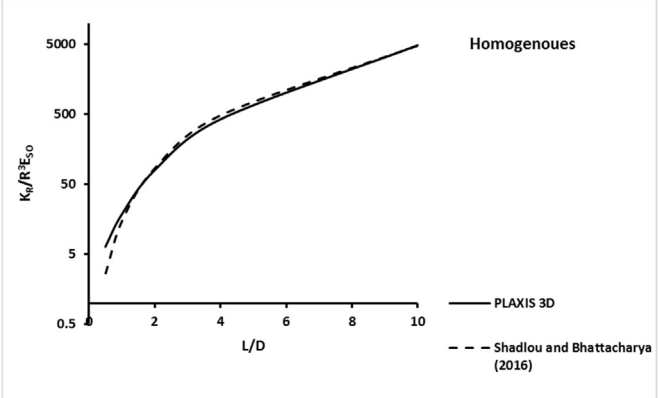

A.4 Obtaining the natural frequency

Step 1. (Fixed Based Natural Frequency of the Tower).
Calculate the bending stiffness ratio of Tower to the pile

$$\chi = \frac{E_T I_T}{E_P I_P}$$

Calculate the platform/tower length ratio

$$\psi = \frac{L_s}{L_T}$$

Calculate the substructure flexibility co-efficient to account for the enhanced stiffness of the Transition piece

$$C_{MP} = \sqrt{\frac{1}{1 + (1+\psi^3)\chi - \chi}}$$

Obtain the fixed base natural frequency of the tower

$$f_{FB} = \frac{1}{2\pi} C_{MP} \sqrt{\frac{3E_T I_T}{\left(mRNA + \frac{33mT}{140}\right) {L_T}^3}}$$

Where the cross-sectional properties of the tower can be calculated as

$$D_T = \frac{D_b + D_t}{2} \quad I_T = \frac{1}{8}(D_T - t_T)^3 t_T \pi$$

Step 2. Calculate the non-dimensional foundation stiffness parameters
The equivalent bending stiffness of tower needed for this step:

$$q = \frac{D_b}{D_T} \quad f(q) = \frac{1}{3} \times \frac{2q^2(q-1)^3}{2q^2 \ln q - 3q^2 + 4q - 1} \quad EI_\eta = EI_{top} \times f(q)$$

Where I_{top} is the second moment of area of the top section of the tower

$$\eta_L = \frac{K_L L^3}{EI_\eta}$$

$$\eta_{LR} = \frac{K_{LR} L^2}{EI_\eta}$$

$$\eta_R = \frac{K_R L}{EI_\eta}$$

Step 3. Calculate the foundation flexibility factors

$$C_R(\eta_L, \eta_{LR}, \eta_R) = 1 - \frac{1}{1 + 0.6\left(\eta_R - \frac{\eta^2_{LR}}{\eta_L}\right)}$$

$$C_L(\eta_L, \eta_{LR}, \eta_R) = 1 - \frac{1}{1 + 0.5\left(\eta_L - \frac{\eta^2_{LR}}{\eta_R}\right)}$$

Step 4. Calculate the flexible natural frequency of the OWT system

$$f_0 = C_L C_R f_{FB}$$

Numerical Example:

$$D_T = \frac{3.87+6}{2} = 4.935m \quad I_T = \frac{1}{8}(4.935-0.027)^3 \times 0.027 \times \pi = 1.25m^4$$

$$\chi = \frac{210 \times \pi \times (4.935-0.027)^3 \times 0.027/8}{210 \times \pi \times (6-0.027)^3 \times 0.027/8} = 0.55$$

$$\psi = \frac{30}{87.6} = 0.34$$

$$C_{MP} = \sqrt{\frac{1}{1+(1+0.34)^3 \times 0.55 - 0.55}} = 0.75$$

$$f_{FB} = \frac{1}{2\pi} \times 0.75 \times \sqrt{\frac{3 \times 210E9 \times 1.25}{(350000 + \frac{33 \times 347460}{140})87.6^3}} = 0.21Hz$$

The fixed base frequency is therefore 0.26 Hz.

$$q = \frac{6}{3.87} = 1.55 \quad f(q) = \frac{1}{3} \times \frac{2 \times 1.55^2(1.55-1)^3}{2 \times 1.55^2 \ln 1.55 - 3 \times 1.55^2 + 4 \times 1.55 - 1} = 2.71$$

$$EI_\eta = 210 \times \frac{1}{8}(3.87-0.027)^3 \times 0.027 \times \pi \times 2.71 = 342GPa$$

The non-dimensional groups are:

$$\eta_L = \frac{0.86 \times 87.6^3}{342} = 1690 \quad \eta_{LR} = \frac{-3.5 \times 87.6^2}{342} = -78 \quad \eta_R = \frac{44 \times 87.6}{342} = 11$$

The foundation flexibility coefficients are given as follows:

$$C_R(\eta_L, \eta_{LR}, \eta_R) = 1 - \frac{1}{1+0.6\left(11 - \frac{-78^2}{1690}\right)} = 0.82 \quad C_L(\eta_L, \eta_{LR}, \eta_R) = 1 - \frac{1}{1+0.5\left(1690 - \frac{-78^2}{11}\right)} = 0.999$$

The natural frequency is therefore given by:

$$f_0 = 0.82 \times 0.999 \times 0.26 = 0.17Hz$$

References

Abbas, J.M., Chik, Z.H., Taha, M.R., 2008. Single pile simulation and analysis subjected to lateral load. Electron. J. Geotech. Eng. 13.

Adhikari, S., Bhattacharya, S., 2012. Dynamic analysis of wind turbine towers on flexible foundations. Shock Vib. 19, 37–56.

Aldridge, T., Carrington, T., Kee, N., 2005. Propagation of pile tip damage during installation. In: Gourvenec, S., Cassidy, M. (Eds.), Proc. Int. Conf. Frontiers in Offshore Geotechnics. Taylor and Francis, p. 827.

Arany, L., Bhattacharya, S., MacDonald, J., Hogan, S.J., 2017. Design of monopiles for offshore wind turbines in 10 steps. Soil Dynam. Earthq. Eng. 92, 126–152.

Arany, L., Bhattacharya, S., MacDonald, J.H., Hogan, S.J., 2016. Closed form solution of Eigen frequency of monopile supported offshore wind turbines in deeper waters incorporating stiffness of substructure and SSI. Soil Dynam. Earthq. Eng. 83, 18–32.

Arany, L., Bhattacharya, S., Adhikari, S., Hogan, S.J., MacDonald, J.H.G., 2015. An analytical model to predict the natural frequency of offshore wind turbines on three-spring flexible foundations using two different beam models. Soil Dynam. Earthq. Eng. 74, 40–45.

Bhattacharya, S., 2013. Challenges in design of foundations for offshore wind turbines. Eng. Technol. Ref. 1–9.

Bhattacharya, S., Carrington, T., Aldridge, T., 2005. Buckling considerations in pile design. In: Proceedings of the International Symposium on Frontiers in Offshore Geotechnics, pp. 815–821.

Bhattacharya, S., Wang, L., Liu, J., Hong, Y., 2017. Civil engineering challenges associated with design of offshore wind turbines with special reference to China. In: Wind Energy Engineering: a Handbook for Onshore and Offshore Wind Turbines. Elsevier.

Carter, J., Kulhawi, F., 1992. Analysis of laterally loaded shafts in rock. J. Geotech. Eng. 118, 839–855.

Cox, J.A., Bhattacharya, S., 2016. Serviceability of suction caisson founded offshore structures. In: Proceedings of the Institution of Civil Engineers-geotechnical Engineering, pp. 1–12.

Doherty, J., Houlsby, G., Deeks, A., 2005. Stiffness of flexible caisson foundations embedded in nonhomogeneous elastic soil. J. Geotech. Geoenviron. Eng. 131, 1498–1508.

Gazetas, G., 1983. Analysis of machine foundations: state of the art. Soil Dynam. Earthq. Eng. 2, 2–42.

Gazetas, G., 1991. Formulas and Charts for impedances of surface and embedded foundations. J. Geotech. Eng. 1129–1141.

Gelagoti, F., Lekkakis, P., Kourkoulis, R., Gazetas, G., 2015. Estimation of elastic and non-linear stiffness coefficients for suction caisson foundations. In: Geotechnical Engineering for Infrastructure and Development. ICE.

Gibson, R., 1974. The analytical method in soil mechanics. Geotechnique 24, 115–140.

Golightly, C., 2014. Tilting of monopiles long, heavy and stiff; pushed beyond their limits. Tech. Note Ground Eng. 20–23. https://www.geplus.co.uk/Journals/2014/06/03/z/h/d/GE-January-2014-Tilting-of-monopiles-Golightly.pdf.

Higgins, W., Basu, D., 2011. Fourier Finite Element Analysis of Laterally Loaded Piles in Elastic Media. Internal Geotechnical Report 2011-1. University of Connecticut, Connecticut, US.

Houlsby, G.T., Ibsen, L.B., Byrne, B.W., 2005. Suction caissons for wind turbines. In: CASSIDY, G. (Ed.), Frontiers in Offshore Geotechnics: ISFOG. Taylor & Francis Group, London.

Jalbi, S., Shadlou, M., Bhattacharya, S., 2017. Practical method to estimate foundation stiffness for design of offshore wind turbines. In: Wind Energy Engineering: a Handbook for Onshore and Offshore Wind Turbines. Elsevier.

Jonkman, J., Butterfield, S., Musial, W., Scott, G., 2009. Definition of a 5-MW Reference Wind Turbine for Offshore System Development. National Renewable Energy Laboratory, technical Report No. NREL/TP-500-38060. U.S department of Energy, Golden, CO.

Krishnaveni, B., Alluri, S.K.R., Murthy, M.R., 2016. Generation of p-y curves for large diameter monopiles through numerical modelling. Int. J. Renew. Energy Technol. 5 (7), 379–388.

Latini, C., Zania, V., 2017. Dynamic lateral response of suction caissons. Soil Dynam. Earthq. Eng. 100, 59–71. https://www.sciencedirect.com/science/article/pii/S0267726117301823.

Müller, A., Zerbs, C., 2011. Offshore Wind Farms-Measuring Instruction for Underwater Sound Monitoring. Report/protocol for Bundesamt Fur Seeschifffahrt und Hydrographie. Germany.
Poulos, H., Davis, E., 1974. Elastic Solution for Soils and Rock Mechanics. John Wiley & Sons, New York.
Randolph, M., 1981. The response of flexible piles to lateral loading. Geotechnique 31, 247–259.
Shadlou, M., Bhattacharya, S., 2016. Dynamic stiffness of monopiles supporting offshore wind turbine generators. Soil Dynam. Earthq. Eng. 88, 15–32.
Stroescu, I., Frigaard, P., Fejeskov, M., 2016. Scour development around bucket foundations. Int. J. Polar Offshore Eng. 26, 57–64.
Whitehouse, R., 2004. Marine scour at large foundations. In: Second International Conference on Scour and Erosion (ICSE-2). Singapore.